Wind turbine power coefficient models based on neural networks and polynomial fitting

Miguel Carpintero-Renteria[1] ✉, David Santos-Martin[1], Andrew Lent[2], Carlos Ramos[1]

[1]Department of Electrical Engineering, University Carlos III of Madrid (UC3M), Calle de Butarque 15, 28912, Spain

[2]University of Maryland, College Park, MD 20742, USA

✉ *E-mail: micarpin@ing.uc3m.es*

Abstract: The power coefficient parameter represents the aerodynamic wind turbine efficiency. Since the 1980s, several equations have been used in the literature to study the power coefficient as a function of the tip speed ratio and the pitch angle. In this study, these equations are reviewed and compared. A corrected blade element momentum algorithm is used to generate three sets of data representing different ranges of wind turbines, going from 2 to 10 MW. With this information, two power coefficient models are proposed and shared. One model is based on a polynomial fitting, whereas the other is based on neural network techniques. Both were trained with the blade element momentum model output data and showed good behaviour for all operating ranges. In the results, compared to all the algorithms found in the literature, the proposed models reduced the power coefficient error by at least 55% compared to the best numerical approximation from the literature. An error reduction in the power coefficient parameter may have a large impact on many wind energy conversion system studies, such as those treating dynamic and transient behaviours.

1 Introduction

There are a number of different methods that can be used and perspectives that can be taken when modelling a wind energy conversion system (WECS). The effect of aggregated wind turbines can be studied by developing wind farm models. Similarly, single wind turbine models can be developed to study the influence of a single machine. The impact of each of the different components or subsystems within a wind turbine can also be modelled.

Since wind energy is usually provided by wind farms, some authors developed mathematical models taking into account all the wind turbines in the farm [1–3]. For instance, Conroy and Watson [1] used a mechanical, electrical, and electronic model of the wind turbine to study the transient stability between the wind farm and the power system. Using a similar approach, Di Fazio and Russo [2] modelled a wind farm for reliability assessment purposes with the grid. According to them, there are no simplifications for the wind data or the wind turbine characteristics. Although Zou *et al*. [3] mainly focused on wind farm modelling, they analysed a single machine with three subsystems: wind speed, wind turbine, and transmission and generator models. To speed up simulations, many simplifications are typically applied when modelling a wind farm.

Table 1 Wind turbine subsystem models covered by the studies

Studies	Wind model	Blades model	Drive-train model	Generator/ electric model	Converter model
[6]		✓		✓	
[7]		✓	✓		
[8]		✓			
[5]				✓	
[9]			✓		
[10]		✓		✓	
[11]		✓	✓	✓	
[12]			✓	✓	✓
[13]	✓	✓	✓	✓	
[14]		✓	✓	✓	
[15]			✓	✓	
[16]	✓	✓	✓	✓	
[3]	✓		✓	✓	
[17]		✓			
[18]			✓	✓	✓
[19]		✓		✓	✓
[20]			✓	✓	✓
[21]			✓		

Conversely, single wind turbine models are frequently more detailed than wind farm models. MOD-2 was, in the very early stages, a wind turbine model with two blades for simulation purposes. According to Anderson and Bose [4], this model had problems, but none without resolution. In the same paper, the basic subsystems a wind turbine model should cover were mentioned. These subsystems, along with other common ones, are listed in Table 1. Among the reviewed models, the model proposed by Lee *et al*. [5] is the only data-driven model. This means that by implementing different types of neural networks (NNs), active and reactive power output was obtained from the following data inputs: three-phase voltages and rotor speed. Data-driven methods may avoid using deterministic equations to obtain the desired result, while the other models were developed with mathematical equations trying to replicate the physical behaviour of the wind turbines.

Among the wind turbine subsystem models from Table 1, this study is mainly focused on the blades model and, more specifically, on the turbine's power coefficient C_p. A common method for finding the C_p of a turbine under a variety of operating conditions is to use the blade element momentum theory (BEM) [22]. To find the C_p, a BEM algorithm will generally implement a variety of correction factors to account for three-dimensional aerodynamic effects that occur under normal operating conditions and that are not included in classical BEM theory [22]. With the inclusion of these correction factors, many early BEM algorithms suffered from numerous regions of non-convergence where the algorithm would fail to converge due to an initial flow condition. For this reason and due to the extreme variety of correction factors that can be utilised, for this study, the robust algorithm used by AeroDyn and proposed in [23] was chosen. The use of such an algorithm allows for a comprehensive study of the full range of each turbine's operating

Table 2 Exponential power coefficient equations

Studies	C_p	λ_i	Equation
[24–28]	$C_p(\lambda,\beta)=0.5176(\frac{116}{\lambda_i}-0.4\beta-5)e^{\frac{-21}{\lambda_i}}+0.0068\lambda$	$\frac{1}{\lambda_i}=\frac{1}{\lambda+0.08\beta}-\frac{0.035}{\beta^3+1}$	(1)
[29]	$C_p(\lambda,\beta)=0.5109(\frac{116}{\lambda_i}-0.4\beta-5)e^{\frac{-21}{\lambda_i}}+0.0068\lambda$	$\frac{1}{\lambda_i}=\frac{1}{\lambda+0.08\beta}-\frac{0.0035}{\beta^3+1}$	(2)
[14, 25, 29–31]	$C_p(\lambda,\beta)=0.73(\frac{151}{\lambda_i}-0.58\beta-0.002\beta^{2.14}-13.2)e^{\frac{-18.4}{\lambda_i}}$	$\frac{1}{\lambda_i}=\frac{1}{\lambda-0.02\beta}-\frac{0.003}{\beta^3+1}$	(3)
[25]	$C_p(\lambda,\beta)=(\frac{110}{\lambda_i}-0.4\beta-0.002\beta^{2.2}-9.6)e^{\frac{-18.4}{\lambda_i}}$	$\frac{1}{\lambda_i}=\frac{1}{\lambda+0.02\beta}-\frac{0.03}{\beta^3+1}$	(4)
[25, 32–37]	$C_p(\lambda,\beta)=0.5(\frac{116}{\lambda_i}-0.4\beta-5)e^{\frac{-21}{\lambda_i}}$	$\frac{1}{\lambda_i}=\frac{1}{\lambda+0.08\beta}-\frac{0.035}{\beta^3+1}$	(5)
[25]	$C_p(\lambda,\beta)=0.5(\frac{116}{\lambda_i}-0.4\beta-5)e^{\frac{-21}{\lambda_i}}$	$\frac{1}{\lambda_i}=\frac{1}{\lambda+0.088}-\frac{0.035}{\beta^3+1}$	(6)
[6, 25, 29, 38]	$C_p(\lambda,\beta)=0.22(\frac{116}{\lambda_i}-0.4\beta-5)e^{\frac{-12.5}{\lambda_i}}$	$\frac{1}{\lambda_i}=\frac{1}{\lambda+0.08}-\frac{0.035}{\beta^3+1}$	(7)
[39]	$C_p(\lambda,\beta)=0.39(\frac{116}{\lambda_i}-0.4\beta-5)e^{\frac{-16.5}{\lambda_i}}$	$\frac{1}{\lambda_i}=\frac{1}{\lambda+0.089\beta}-\frac{0.035}{\beta^3+1}$	(8)
[25]	$C_p(\lambda,\beta)=0.5(\frac{72.5}{\lambda_i}-0.4\beta-5)e^{\frac{-13.125}{\lambda_i}}$	$\frac{1}{\lambda_i}=\frac{1}{\lambda+0.08\beta}-\frac{0.035}{\beta^3+1}$	(9)
[25]	$C_p(\lambda,\beta)=0.44(\frac{124.99}{\lambda_i}-0.4\beta-6.94)e^{\frac{-17.05}{\lambda_i}}$	$\frac{1}{\lambda_i}=\frac{1}{\lambda+0.08\beta}-\frac{0.001}{\beta^3+1}$	(10)

Table 3 Sinusoidal power coefficient equations

Studies	C_p	Equation
[25, 40–42]	$C_p(\lambda,\beta)=(0.44-0.0167\beta)\sin\left(\frac{\frac{\pi}{2}(\lambda-3)}{7.5-0.15\beta}\right)-(\lambda-3)(0.00184\beta)$	(11)
[25, 29]	$C_p(\lambda,\beta)=(0.5+0.167(\beta-2))\sin\left(\frac{\pi(\lambda+0.1)}{18.5-0.3(\beta-2)}\right)-0.00184(\lambda-3)(\beta-2)$	(12)
[25]	$C_p(\lambda,\beta)=(0.5-0.00167(\beta-2))\sin\left(\frac{\pi(\lambda+0.1)}{18.5-0.3(\beta-2)}\right)+0.00184(\lambda-3)(\beta-2)$	(13)
[25]	$C_p(\lambda,\beta)=(0.5-0.0167(\beta-2))\sin\left(\frac{\pi(\lambda+0.1)}{10-0.3\beta}\right)-0.00184(\lambda-3)(\beta-2)$	(14)

conditions without diverting attention to the development of a novel BEM algorithm.

In the past, various numerical models have been proposed to calculate the C_p of a wind turbine as a function of λ, β. In this study, issues with the accuracy of those models in modern turbines are discussed and the data gathered from the BEM algorithm proposed in [23] is used to develop two new numerical approximations. The proposed C_p models can be used in the static analysis, such as power production, although its main application may be related to dynamic studies such as testing control systems (such as those related to pitch, power electronics etc.) or integration studies (such as inertia simulation, frequency control etc.).

The paper is structured as follows. In Section 2, a review of the different numerical approaches used in the literature to calculate the power coefficient is presented. Then, a study of previous BEM works is provided and a new one with a special focus on correlation parameters is proposed in Section 3. Section 4 shows the development of two proposed C_p models and the data used for them. A comparison between all of the described C_p described models is provided in Section 5. Conclusions are explained and discussed in Section 6.

2 Review of recent power coefficient models

In this section, a literature review of different numerical approximations of C_p is introduced. First, the C_p concept is presented. Then, different algorithms are explained, referenced, and gathered into tables. All numerical approximations shown in Tables 2 and 3 are compared with the proposed models in Section 5.

The power coefficient, called the performance coefficient by some authors [6, 24, 30, 32, 40], stands for the aerodynamic turbine efficiency, which differs from one type of wind turbine to another. The introduction of the C_p concept was made in the one-dimensional momentum theory, in which a theoretical power coefficient limit of around $C_p\max = 0.59$ for two-blade or three-blade horizontal axis wind turbines was defined by using [43]. When considering a more detailed angular momentum balance, the power coefficient is a function of the tip speed ratio (TSR) (λ) and the pitch angle (β), $C_p(\lambda,\beta)$ [44]. The TSR mathematical expression is defined in (15), where w_t is the turbine rotational speed, R is the turbine radius and v_w is the wind speed. In exponential equations, the parameter λ_i functions on the instantaneous parameters of (λ,β)

$$\lambda=\frac{w_t R}{v_w} \tag{15}$$

There are different techniques for modelling the C_p. These algorithms can be differentiated into exponential, sinusoidal, polynomial, or data-driven algorithms. In [25], the researchers made a similar cluster of these algorithms along with a formula generalisation for each type except for data-driven algorithms, which were not included.

In the literature reviewed, the power coefficient model based on exponential equations has more variations than any other. A general equation of this type of algorithm was made by Reyes *et al*. [25]. In Table 2, all the exponential equations found in the literature are shown. To the best of the author's knowledge, the oldest equation is shown in [33] and corresponds to (5). This equation was developed by Wasynczuk *et al*. [34] with a least-square fitting using the manufacturer's model MOD-2 wind turbine, the characteristics of which can be found in the same reference. Slootweg *et al*. [32] slightly modified the coefficients of the C_p with multidimensional optimisation to exhibit better behaviour of the model compared with their manufacturer data. Also, different coefficient numbers were used with constant and variable speeds. From (5) to (10), the pitch angle is considered in degrees and the structure of the equations is the same, but with different coefficients to fit each research paper's purpose.

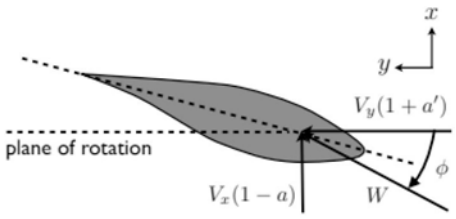

Fig. 1 *BEM velocity triangle*

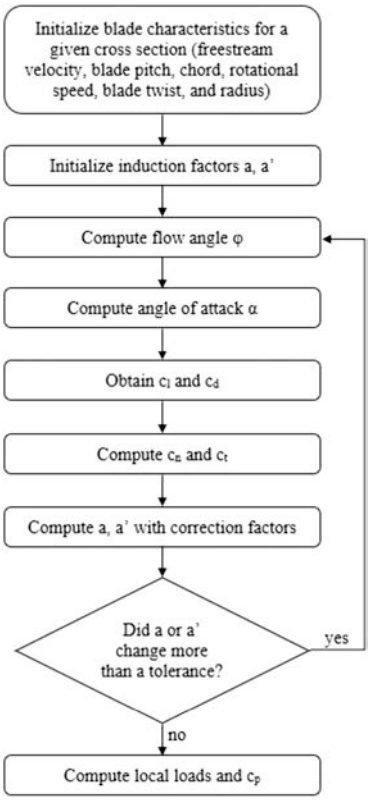

Fig. 2 *BEM algorithm*

Equations (3) and (4) add the same quadratic coefficient, while most of the other constants are changed. Another difference among them is with the term λ_i. In (1) and (2), a new constant is added multiplying the TSR variable into account.

Few algorithms have been created with regard to sinusoidal equations. In Table 3, the equations used in different studies are presented and they have noticeable similarities. The pitch angle must be considered in degrees. The 14 equations found in the literature are tested in Section 5 and compared with our proposed models.

In [25], polynomial equations are reviewed. None of them are used in this study since the power coefficient is shown as a function of TSR only. Nevertheless, there is a polynomial approximation of the C_p taking both variables into account shown in [45]. This algorithm is built from the approximation of two concrete wind turbines of 1.5 and 3.6 MW. An approximation test dataset has been generated with this model to compare all the algorithms from Tables 2 and 3 and the models created with the manufacturer's wind turbine data. Those results are shown in Section 5.

Regarding data-driven algorithms, in [46], two ways to calculate the C_p are proposed: one is based on statistical data and the other is based on real-time data. According to the authors, the model generated with statistical data is worth using to define the performance of the wind turbine, whereas the model based on real-time data may have better performance with wind turbine dynamic control. Machine learning techniques are not widely used in the literature for C_p calculations. In [47], an adaptive neuro-fuzzy inference system is proposed as a model to obtain the C_p out of the pitch and TSR. This model is developed with information from an offshore wind turbine from NREL with a nominal power of 5 MW. The simulation model was designed and tested with the experimental data from that wind turbine, but no generalisation and test with other machines have been developed. Nevertheless, the algorithm seems to have a good performance within the characteristics of the wind turbine.

3 Blade element momentum model

The BEM theory unifies blade element theory and momentum theory, synthesised in Figs. 1 and 2. The implemented BEM algorithm can be found in [23].

The lift and drag coefficients of the aerodynamic profiles are calculated with 2D and 3D simulations at different angles of attack and at a fixed Reynolds number, due to the negligible influence on the polar data at $Re > 10^6$ (typical order in wind turbines operation) [48]. Two corrections are applied to the BEM: the momentum theory breakdown and the hub-tip loss. To assure the validity of the code for high axial induction factors and overcome the momentum theory breakdown, the Glauert correction with Buhl's modification is applied [49]. The second correction corresponds to the Prandtl's hub/tip loss correction, used to take into account the difference between a rotor of a finite and infinite number of blades together with the effect of the hub-vortexes generation [22].

The axial (a) and the tangential (a') induction factors represent the relationship between the induction (U_x, U_y) and free upstream velocities (V_x, V_y) [22], represented in Fig. 1 and calculated as

$$U_x = V_x(1-a) \tag{16}$$

$$U_y = V_y(1+a') \tag{17}$$

The axial and tangential parameters needed in the algorithm (K and K') are calculated as

$$K = \frac{\sigma' c_x}{4F\sin^2\phi} \tag{18}$$

$$K' = \frac{\sigma' c_y}{4F\sin\phi\cos\phi} \tag{19}$$

The induction factors (a, a') are obtained depending on the momentum region. If $\phi > 0$ and $K < 2/3$, then the axial induction factor is

$$a = \frac{K}{1+K} \tag{20}$$

Alternatively, if $\phi > 0$ and $K > 2/3$, then

$$a = \frac{\gamma_1 - \sqrt{\gamma_2}}{\gamma_3} \tag{21}$$

where

$$\gamma_1 = 2FK - (10/9 - F)$$
$$\gamma_2 = 2FK - F(4/3 - F)$$
$$\gamma_3 = 2FK - (25/9 - 2F)$$

The tangential induction factor calculation is common for both regions

$$a' = \frac{K'}{1-K'} \tag{22}$$

The parameter of interest is the power coefficient, which is defined as the power extracted from the turbine with respect to the total possible extracted power from the air

$$C_p = \frac{P}{\frac{1}{2}\rho A V_x^3} \tag{23}$$

Table 4 C_p polynomial coefficients

i	j	$K_{i,j}$	(95% confidence bounds)
0	0	0.244	(0.239, 0.2489)
1	0	−0.3744	(0.38, −0.3689)
0	1	−0.03344	(−0.03416, −0.03272)
2	0	0.1827	(0.1805, 0.1849)
1	1	0.03828	(0.03769, 0.03887)
0	2	0.0009145	(0.0007963, 0.001033)
3	0	−0.0295	(−0.02989, −0.02911)
2	1	−0.01085	(−0.011, −0.01069)
1	2	−0.0006625	(−0.0007255, −0.0005994)
0	3	-1.539×10^{-5}	$(-2.669 \times 10^{-5}, -4.093 \times 10^{-6})$
4	0	0.002036	(0.002005, 0.002068)
3	1	0.001118	(0.001101, 0.001135)
2	2	8.23×10^{-5}	$(7.266 \times 10^{-5}, 9.194 \times 10^{-5})$
1	3	-1.175×10^{-5}	$(-1.507 \times 10^{-5}, -8.425 \times 10^{-6})$
0	4	1.982×10^{-6}	$(1.487 \times 10^{-6}, 2.476 \times 10^{-6})$
5	0	-5.193×10^{-5}	$(-5.291 \times 10^{-5}, -5.096 \times 10^{-5})$
4	1	-3.721×10^{-5}	$(-3.781 \times 10^{-5}, -3.66 \times 10^{-5})$
3	2	-8.369×10^{-6}	$(-8.808 \times 10^{-6}, -7.931 \times 10^{-6})$
2	3	1.139×10^{-6}	$(9.021 \times 10^{-7}, 1.376 \times 10^{-6})$
1	4	4.356×10^{-7}	$(3.788 \times 10^{-7}, 4.924 \times 10^{-7})$
0	5	-6.631×10^{-8}	$(-7.449 \times 10^{-8}, -5.812 \times 10^{-8})$

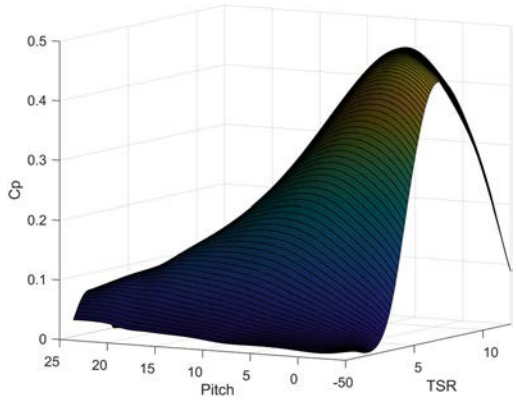

Fig. 3 *Polynomial surface of the $C_p(\lambda, \beta)$*

The BEM algorithm is summarised in Fig. 2. The entire block diagram is looped through for each cross-section on the blade at every TSR and pitch value in the operating regime.

4 Data used and proposed models

This section is divided into two parts. First, the data used to develop the power coefficient algorithms and compare the models in Section 5 are explained. Then, two different models are proposed. One is based on polynomial algorithms, and the other based on data-driven techniques such as NNs.

4.1 Data

There are two purposes when using the data in this study. First, the aerodynamic details of different wind turbines are used to generate, through the BEM, a C_p surface as a function of TSR and pitch. The second purpose is to have three different wind turbine surfaces to test and compare the models proposed with the numerical approximations found in the literature.

Regarding the input data for the BEM, three wind turbines are used in the scope of the analysis: the Tjaereborg 2 MW, the NREL 5 MW, and the DTU 10 MW. The NREL 5 MW [50] and the DTU 10 MW [51, 52] are modern turbines developed in the 21st century by research institutions, which provide access to the geometric and performance data. The Tjaereborg machine represents the wind turbine technology of the early 1980s [53, 54]. Each of the three wind turbines analysed in this study has unique blade structures. To model these structures, each blade was discretised into numerous parts, with each section being represented by a specific airfoil. To generate the C_p data for each turbine, 3D corrected aerodynamic data was used for every airfoil that made up each blade.

The BEM is run for the three turbines using a wide range of pitch angles (β) and TSR (λ) values to generate a surface that provides the power coefficient. The range is selected to coincide with the typical operating conditions of a wind turbine. One surface for each type of wind turbine is generated and used to fit the two different power coefficient models in Section 4.2. These models are designed to cover a wind turbine range among the input data used as the BEM input.

In Section 5, a test dataset made with three different types of wind turbines is used. Two of them have been shared by different companies to develop this study, but due to confidentiality agreements, only the power capacity and the wind turbine diameters are shown. The smallest wind turbine has a nominal power of 0.85 MW and a diameter of 52 m. The acronym WT1 is used to refer to this wind turbine. The second wind turbine has a nominal power of 1.2 MW and a diameter of 90 m. It is labelled WT2.

To cover a wider range of examples in the test, a third set of data was produced out of the numerical C_p model of [45]. This polynomial algorithm is made out of two wind turbines, one with a nominal power of 1.5 MW and the other of 3.6 MW. No diameters were specified for these turbines. By giving the polynomial a typical operating range of TSR and pitch values, the power coefficient was obtained. This third data test set is named WT3.

4.2 Power coefficient proposed models

Two different power coefficient models are proposed. One is based on a polynomial fitting, and the other is based on NN techniques. Both models were generated using MATLAB coding. Whereas the polynomial algorithm and equation are given in this section, the NN model is shared through a GitHub link with the entire MATLAB code.

4.2.1 Polynomial model: This algorithm has been developed by gathering the three BEM output sets of data into a matrix with three columns that correspond to the TSR, pitch, and C_p values. With this set of data, a fitting function was implemented. Different polynomial orders were studied. For instance, the fourth-order algorithm had much better results than the third-order algorithm. In contrast, the fifth-order algorithm had a slightly better result than the fourth-order algorithm. The improvement of the sixth-order algorithm was even less. To have a compromise between accuracy and complexity, fifth-order was chosen as the polynomial order. The structure of the algorithm is shown in (24)

$$C_p(\lambda, \beta) = \sum_{i=0}^{5} \sum_{j=0}^{5} K_{i,j} \lambda^i \beta^j \tag{24}$$

The fifth-order polynomial coefficients ($K_{i,j}$) were found by using linear least square regression. With this method, the summed squared error of residuals is minimised and hence the coefficients in the polynomial fitted to be as similar to the input data surface from the BEM algorithm as possible. The obtained values for each polynomial constant are displayed in Table 4. All the parameters not shown in the table have no value (equal to zero).

Fig. 3 represents a 3D surface of the polynomial algorithm. In Fig. 4, the power coefficient is also represented but with nine fixed-pitch values and compared only with the TSR parameter.

4.2.2 NN model: NNs are based on biological neurons. Mathematically, these neurons are interconnected units where numerical weights are associated with each interconnection. Each neuron has an input and an output connection. The numerical weights change during a training process, which is an iterative

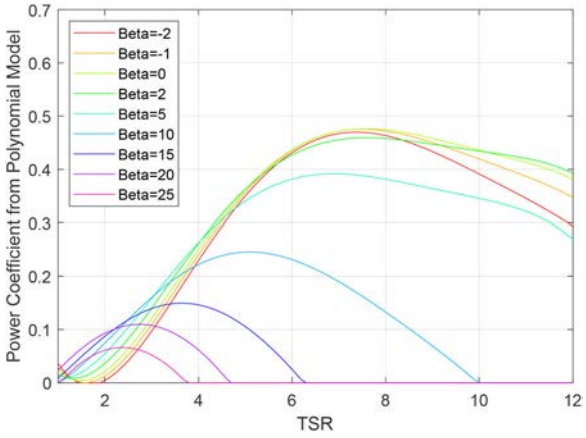

Fig. 4 *C_p values as function of TSR and nine pitch constants of the polynomial model*

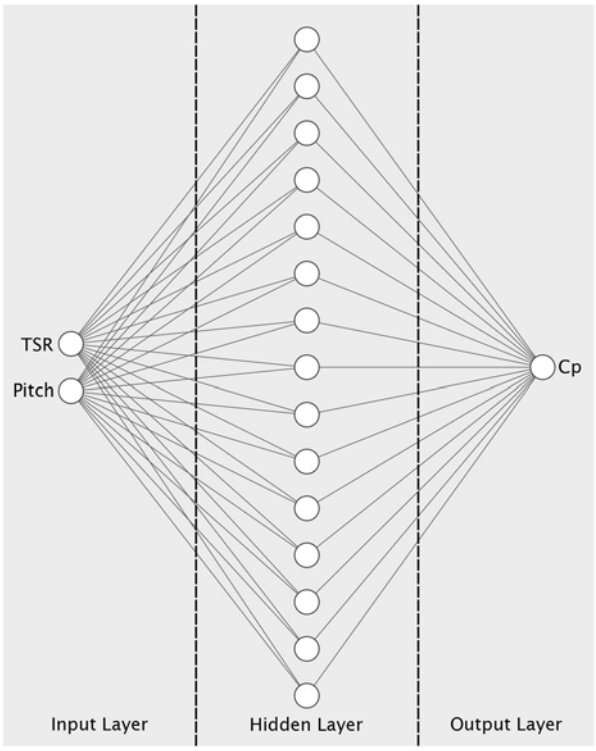

Fig. 5 *NN structure*

mechanism to fit the model to a given dataset [55]. In our NN model, the same training data approach was used with the polynomial model. The matrix with three columns based on BEM outputs is used to train the NN. The data from the matrix is divided randomly into three datasets. Typical splitting percentages of training, validation, and test datasets are 70%, 15%, and15%, respectively. In our model, the entire dataset is used to train the NN since the aim is to fit the BEM output as closely as possible.

NN topology may differ from one project to another. Neurons are gathered into layers, and each NN model may have more than one layer. Layers that are different from the inputs and outputs are called hidden layers. Our NN model has the structure shown in Fig. 5. The proposed model is a non-linear function with two inputs in the input layer. Those inputs are first normalised and then multiplied by the input and output weights of the hidden layer with 15 neurons. Those results go to the output layer, which condenses the information into a single value. Finally, this value is denormalised to obtain the final C_p result. When training the NN, to update each of the weight and bias values, an optimisation according to the Levenberg–Marquardt algorithm was used. The MATLAB training function used was Bayesian regularisation backpropagation [56], and the trained algorithm can be seen at the following link from GitHub (Link).

The NN surface of the power coefficient equation is represented in Fig. 6. Fig. 7 shows the variation of C_p compared to the TSR, with nine fixed-pitch values. Despite being trained with the same dataset, some differences can be found between the polynomial and NN models. In Section 5, both models will be compared using all of the numerical equations from Section 2.

5 Power coefficient models comparison

In this section, a comparison of the power coefficient approximations from Tables 2 and 3 and both proposed models of Section 4.2 is developed. Three wind turbine test sets with different design structures were used to compare the models. The details about these datasets were defined in Section 4.1.

The normalised root mean square error (nRMSE) was the chosen parameter to make comparisons among the models. The nRMSE is represented in (25), where n is the number of parameters in the vector, $\boldsymbol{y}$ is the real data vector and $\hat{y}$ is the vector estimated by the model. The nRMSE is a value per unit, but the table displays it as a percentage for better understanding. All the results of the model comparisons are shown in Table 5. The proposed models have a goodness of fit, measured by the nRMSE, of 4.8% for the polynomial model and 4.2% for the NN model

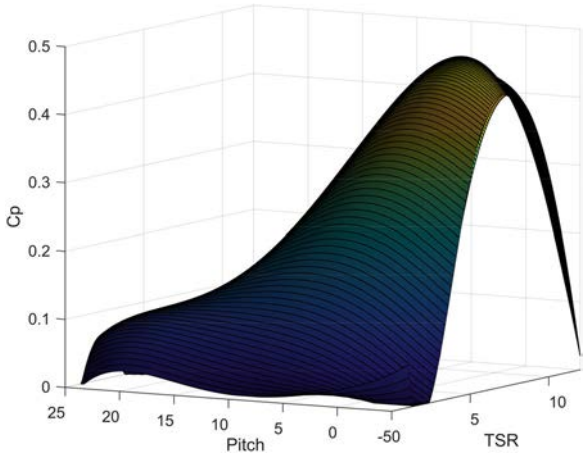

Fig. 6 *NN surface of the $C_p(\lambda, \beta)$*

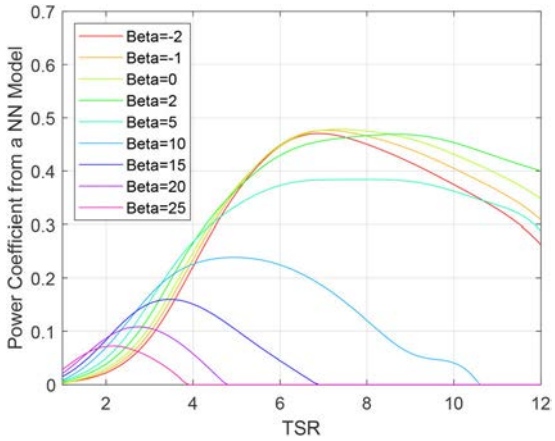

Fig. 7 *C_p values as a function of TSR and nine-pitch constants of the NN model*

Table 5 Comparison of nRMSE percentage value among the power coefficient numerical models

Equations \test set	WT1 nRMSE, %	WT2 nRMSE, %	WT3 nRMSE, %	Mean nRMSE, %
polynomial model	5.8	6.8	5.6	6.1
NN model	5.8	5.3	5.5	5.5
(1)	16.3	17.1	17.6	17
(2)	16.3	17.1	17.7	17
(3)	41.8	47	41.8	43.5
(4)	55.7	65	58.6	59.8
(5)	18.6	19.9	20.4	19.6
(6)	21.2	22.3	22.6	22
(7)	17.4	18.6	17	17.7
(8)	14.5	15.6	15.1	15.1
(9)	36.9	39.7	35.9	37.5
(10)	12.9	14.2	13.5	13.5
(11)	21.2	22	22.1	21.8
(12)	287	275	246	269.3
(13)	51.3	49.3	44.3	48.3
(14)	64.6	67	59.6	63.7

$$\text{nRMSE} = \frac{\sqrt{\frac{\sum_{i=1}^{n} (\hat{y}(i) - y(i))^2}{n}}}{y_{\max} - y_{\min}} \tag{25}$$

Despite the C_p numerical approximations having similar structures, each variant shows very different results. Worth noting is that (12) has an excessive error rate and should be reviewed. The other differences may be caused by the approximations made in each study to fit the wind turbine and study purpose. Actually, in studies [32], with the same equation structure, different coefficients were used for different situations.

The proposed models had very similar results, but with their own benefits. For instance, the polynomial model is easier to understand and has a lower computational cost than the NN model. It has a 54.8% lower error rate than the next best numerical approximation, which is (10). The NN model obtained only a 9.8% lower error rate than the polynomial model. Nevertheless, regarding the best numerical approximation, it obtained an almost 60% lower error rate. The main benefit of a trained NN is that it can be retrained to fit new types of wind turbines instead of starting from scratch. This can allow researchers to make more robust models. Also, if transfer learning approaches are followed, the NN model can be reused for new problems, so less data is utilised for training.

Fig. 8 shows the power coefficient compared with the TSR with four different pitch values. In Fig. 8*a*, the pitch value is set to $\beta = 0$. Fig. 8*b*, it is $\beta = 5$. In Fig. 8*c*, it is $\beta = 10$, and Fig. 8*d*, it is $\beta = 15$. These pitch values have been selected by avoiding the limitations between the numerical approximations and the wind turbine data test sets. For instance, in exponential models, when the pitch value is set to $\beta = -1$, $\lambda_i = 0$ & $C_\text{p} = \infty$. Then, the dataset resolutions of WT1 and WT2 were not the same, and with values of $\beta = -0.5$, where the usually achieved optimal C_p value was unobtainable. The closest value that fitted to all models and test sets was $\beta = 0$. Therefore, steps of five were taken for the β value to represent a wide range of wind turbine situations.

In Fig. 8, the proposed models are compared to the best exponential numerical approximation found in the literature, which corresponds to (10). Continuous lines correspond with the proposed models, whereas the numerical approximation is displayed with different line specifications as per the figure legend. Despite the behaviour with low pitch values being similar, when

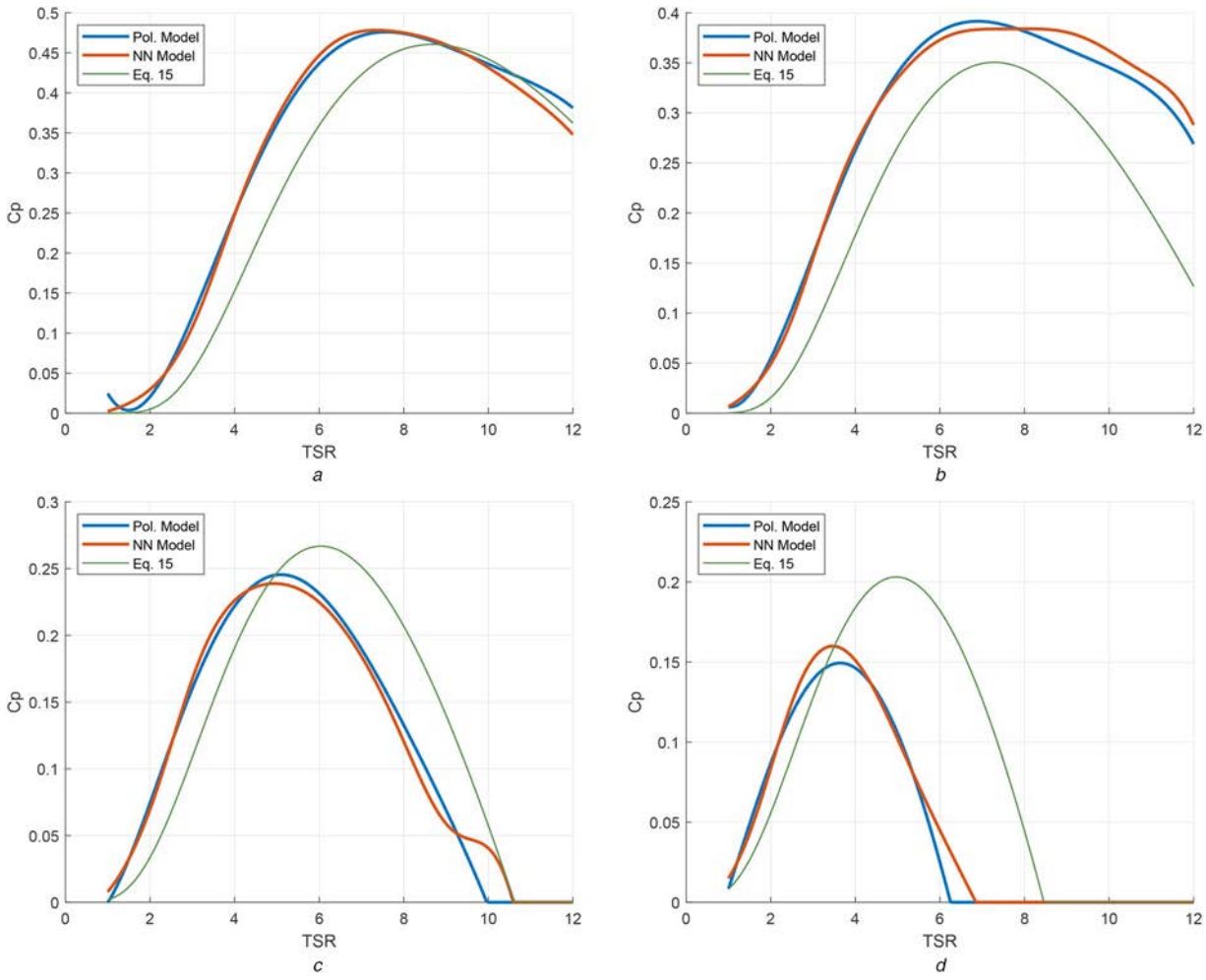

Fig. 8 *C_p values as a function of TSR for the proposed models and the best numerical approximation (10), for some pitch angles:* ***(a)*** *$\beta = 0$,* ***(b)*** *$\beta = 5$,* ***(c)*** *$\beta = 10$;,* ***(d)*** *$\beta = 15$*

this variable increases, the difference between our models and the numerical approximation increases.

In Fig. 9, two different types of numerical approximations are shown. For instance, Figs. 9*a* and *b* display the behaviour between the exponential equations against the proposed models and the data test sets WT1, WT2 and WT3. Fig. 9*c* and *d* show the behaviour of the sinusoidal equations. Both Figs. 9*a* and *c* have a pitch value of $\beta = 0$, whereas Fig. 9*b* and *d* have a pitch value of $\beta = 10$. In Fig. 9*d*, (12) is not visible because it surpassed the power coefficient limit by more than double, and the graph resolution did not properly show the rest of the models. As per the legend, the straight lines correspond to the data test sets, the dashed lines correspond to the proposed models and the dot-dash lines belong to the numerical approximations. Both cases show that the numerical models are more fitted for low pitch values where C_p is higher. Nevertheless, in Fig. 9*a*, a huge dispersion can be seen among the numerical approximations. This dispersion gets even greater when the pitch value increases. Worth noting is that the proposed models, despite being trained with data completely different from the test set, showed quite good behaviour in all situations compared to the numerical approximations. The same thing happens in the sinusoidal numerical approximations, where there is a huge dispersion with $\beta = 0$, but it is even higher with $\beta = 10$. In this case, the numerical approximations obtain at least a 72% lower error rate than the best sinusoidal model. It is worth noting that by using (12) with high pitch values, such as $\beta = 10$, the power coefficient obtained raises above the C_p physical limit established in the theory of Betz.

6 Conclusions

The power coefficient model has been widely used in the body of research in the literature with a similar equation structure since the 1980s. The errors caused on many occasions by this type of approximation may be acceptable for the authors' purposes but as has been shown, it can be significant. This can have a great impact on dynamic and transient studies, so some review of the error implications of this type of equation may be worth examining in future research.

In this study, two power coefficient models have been proposed and tested. Both obtained between 55 and 60% lower error rates than the best numerical approximations found in the literature within this test set. The models were developed with information obtained through a BEM application where three different sets of data were generated to cover a wide range of wind turbine possibilities. Nevertheless, it would be interesting in the future to study more airfoils over a wider variety of wind turbines to further enhance the NN's and polynomial fitting performance. The proposed models obtained goodness-of-fit regarding the BEM output data of 4.8% for the polynomial model and 4.2% for the NN model. The aim of developing the models and sharing them was to obtain good performance when calculating C_p in different types of wind turbines so the models become as universal as possible. These kinds of models can be used for static analysis such as power production. Reducing the error rate in the power coefficient parameter may have a great impact on many WECS studies, such as those treating dynamic and transient behaviours.

The polynomial model has the advantage of having an easy implementation, with good performance and reduced computational cost. The NN model has better performance, with the possibility to retrain it or use it with a transfer learning approach so researchers can make more robust power coefficient algorithms with less input data.

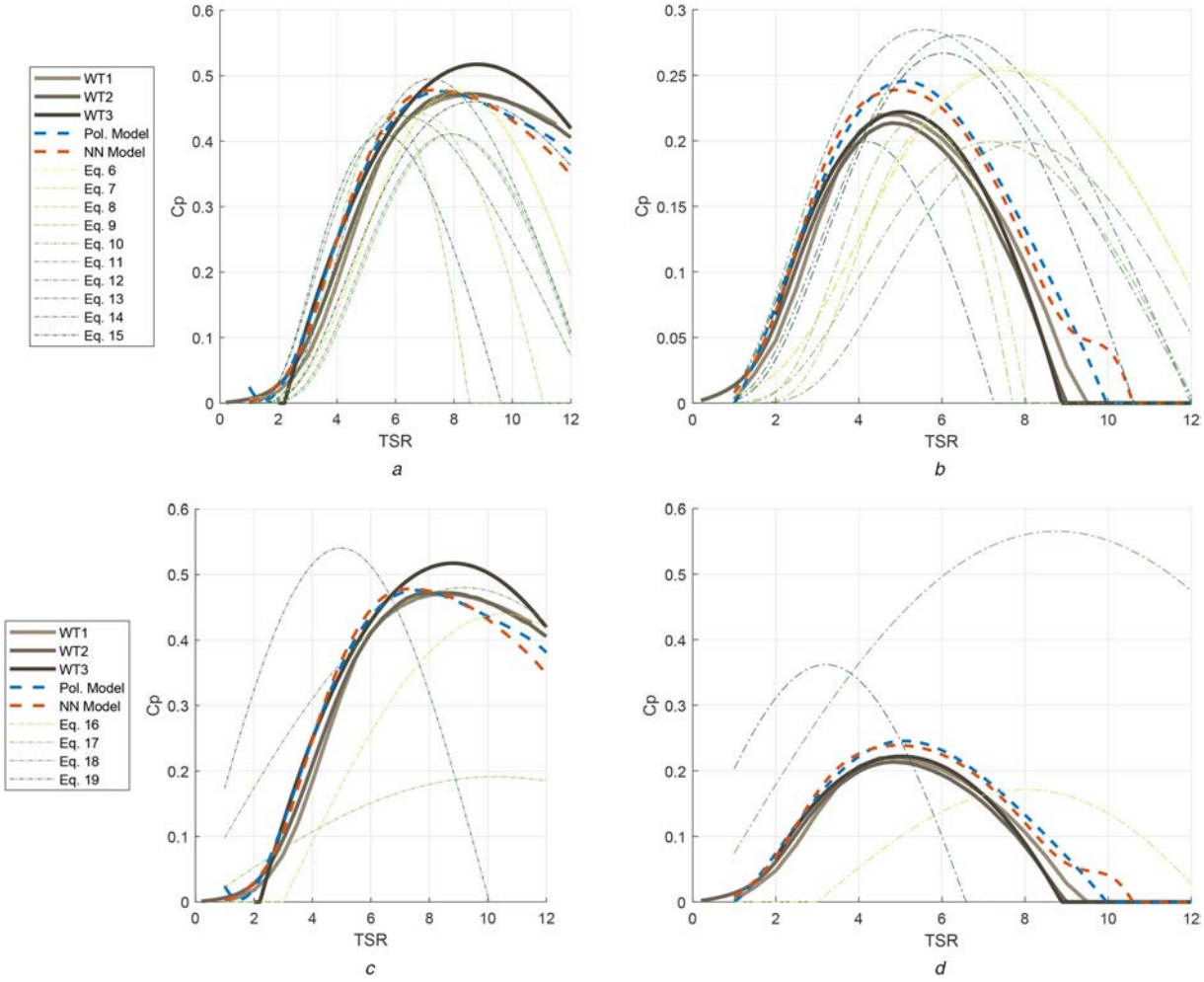

Fig. 9 *C_p values as a function of TSR for the data test set, with the proposed models, the reference models and the literature numerical approximations:* ***(a)*** Models and exponential equations with $\beta = 0$, ***(b)*** Models and exponential equations with $\beta = 10$, ***(c)*** Models and sinusoidal equations with $\beta = 0$; and, ***(d)*** models and sinusoidal equations with $\beta = 10$; $*(12)$ is not shown

7 References

[1] Conroy, J., Watson, R.: 'Aggregate modelling of wind farms containing full-converter wind turbine generators with permanent magnet synchronous machines: transient stability studies', *IET Renew. Power Gener.*, 2009, **3**, (1), pp. 39–52. Available at https://doi.org/10.1049/iet-rpg:20070091

[2] Di Fazio, A., Russo, M.: 'Wind farm modelling for reliability assessment', *IET Renew. Power Gener.*, 2008, **2**, (4), pp. 239–248. Available at https://doi.org/10.1049/iet-rpg:20080005

[3] Zou, J., Peng, C., Yan, Y., *et al.*: 'A survey of dynamic equivalent modeling for wind farm', *Renew. Sust. Energy Rev.*, 2014, **40**, pp. 956–963. Available at https://doi.org/10.1016/j.rser.2014.07.157

[4] Anderson, P., Bose, A.: 'Stability simulation of wind turbine systems', *IEEE Trans. Power Appar. Syst.*, 1983, **12**, pp. 3791–3795

[5] Lee, K.Y., Kong, X., Liu, X.: 'Data-driven modelling of a doubly fed induction generator wind turbine system based on neural networks', *IET Renew. Power Gener.*, 2014, **8**, (8), pp. 849–857, doi: 10.1049/iet-rpg.2013.0391.

[6] Slootweg, J., Polinder, H., Kling, W.: 'Dynamic modelling of a wind turbine with doubly fed induction generator'. 2001 Power Engineering Society Summer Meeting Conf. Proc. (Cat. No. 01CH37262), Vancouver, BC, Canada, 2001, vol. 1, 644–649, doi: 10.1109/PESS.2001.970114. Available at http://ieeexplore.ieee.org/document/970114/

[7] Muyeen, S., Hasan, M., Ali, R., *et al.*: 'Comparative study on transient stability analysis of wind turbine generator system using different drive train models', *IET Renew. Power Gener.*, 2007, **1**, (2), pp. 131–141. doi: 10.1049/iet-rpg:20060030

[8] Manyonge, a.W., Ochieng, R.M., Onyango, F.N.: 'Mathematical modelling of wind turbine in a wind energy conversion system', *Appl. Math. Sci.*, 2012, **6**, (91), pp. 4527–4536

[9] Long, H., Dwyer-Joyce, R.S., Bruce, T.: 'Dynamic modelling of wind turbine gearbox bearing loading during transient events', *IET Renew. Power Gener.*, 2015, **9**, (7), pp. 821–830. doi: 10.1049/iet-rpg.2014.0194

[10] Saleh, S., Khan, M., Rahman, M.: 'Steady-state performance analysis and modelling of directly driven interior permanent magnet wind generators', *IET Renew. Power Gener.*, 2011, **5**, (2), pp. 137. doi: 10.1049/iet-rpg.2010.0054

[11] Lei, T., Ozakturk, M., Barnes, M.: 'Doubly-fed induction generator wind turbine modelling for detailed electromagnetic system studies', *IET Renew. Power Gener.*, 2013, **7**, (2), pp. 180–189. doi: 10.1049/iet-rpg.2012.0222

[12] Hansen, A.D., Michalke, G.: 'Modelling and control of variable-speed multi-pole permanent magnet synchronous generator wind turbine', *Wind Energy*, 2008, **11**, (5), pp. 537–554. doi: 10.1002/we.278

[13] Chen, J., Jiang, D.: 'Study on modeling and simulation of non-grid-connected wind turbine'. WNWEC 2009 – 2009 World Non-Grid-Connected Wind Power and Energy Conf., Nanjing, China, 2009, vol. 2, pp. 292–296. Available at https://doi.org/10.1109/WNWEC.2009.5335791 doi: 10.1109/WNWEC.2009.5335791

[14] Melício, R., Mendes, V.M., Catalão, J.P.: 'Power converter topologies for wind energy conversion systems: integrated modeling, control strategy and performance simulation', *Renew. Energy*, 2010, **35**, (10), pp. 2165–2174. doi: 10.1016/j.renene.2010.03.009

[15] Li, H., Zhao, B., Yang, C., *et al.*: 'Analysis and estimation of transient stability for a grid-connected wind turbine with induction generator', *Renew. Energy*, 2011, **36**, (5), pp. 1469–1476. doi: 10.1016/j.renene.2010.08.023

[16] Baloch, M.H., Wang, J., Kaloi, G.S.: 'Stability and nonlinear controller analysis of wind energy conversion system with random wind speed', *Int. J. Electr. Power Energy Syst.*, 2016, **79**, pp. 75–83. doi: 10.1016/j.ijepes.2016.01.018.

[17] Teow, M.Y., Chiu, H., Tan, R.H.: 'Computational modelling of wind turbine mechanical power and its improve factor determination', 2016

[18] Lorenzo-Bonache, A., Honrubia-Escribano, A., Jiménez-Buendía, F., *et al.*: 'Generic type 3 wind turbine model based on IEC 61400-27-1: parameter analysis and transient response under voltage dips', *Energies*, 2017, **10**, (9), pp. 1–23. doi: 10.3390/en10091441

[19] Torki, W., Grouz, F., Sbita, L.: 'A sliding mode model reference adaptive control of PMSG wind turbine'. Int. Conf. on Green Energy and Conversion Systems GECS 2017, Hammamet, Tunisia, 2017. Available at https://doi.org/10.1109/GECS.2017.8066199 doi: 10.1109/GECS.2017.8066199

[20] Honrubia-Escribano, A., Gómez-Lázaro, E., Fortmann, J., *et al.*: 'Generic dynamic wind turbine models for power system stability analysis: a comprehensive review', *Renew. Sust. Energy Rev.*, 2018, **81**, pp. 1939–1952. doi: 10.1016/j.rser.2017.06.005.

[21] ho Hur, S.: 'Modelling and control of a wind turbine and farm', *Energy*, 2018, **156**, pp. 360–370. doi: 10.1016/j.energy.2018.05.071.

[22] Branlard, E.: '*Wind turbine aerodynamics and vorticity-based methods*' (Springer, Cham, Switzerland, 2017)

[23] Ning, A., Hayman, G., Damiani, R., *et al.*: 'Development and validation of a new blade element momentum skewed-wake model within aerodyn'. 33rd Wind Energy Symp., Kissimmee, Florida, USA., 2015, p. 0215

[24] Muhando, E.B., Senjyu, T., Uehara, A., *et al.*: 'Lqg design for megawatt-class WECS with dfig based on functional models' fidelity prerequisites', *IEEE Trans. Energy Convers.*, 2009, **24**, (4), pp. 893–904

[25] Reyes, V., Rodríguez, J., Carranza, O., *et al.*: 'Review of mathematical models of both the power coefficient and the torque coefficient in wind turbines'. 2015 IEEE 24th Int. Symp. on Industrial Electronics (ISIE) IEEE, Buzios, Brazil, 2015, pp. 1458–1463

[26] Muhando, E.B., Senjyu, T., Uehara, A., *et al.*: 'Gain-scheduled h_∞ control for WECS via LMI techniques and parametrically dependent feedback part I: model development fundamentals', *IEEE Trans. Ind. Electron.*, 2010, **58**, (1), pp. 48–56

[27] Kasiri, H., Abadeh, M.S., Momeni, H.: 'Optimal estimation and control of WECS via a genetic neuro fuzzy approach', *Energy*, 2012, **40**, (1), pp. 438–444

[28] Xia, Y., Ahmed, K.H., Williams, B.W.: 'Wind turbine power coefficient analysis of a new maximum power point tracking technique', *IEEE Trans. Ind. Electron.*, 2012, **60**, (3), pp. 1122–1132

[29] Nouira, I., Khedher, A., Bouallegue, A.: 'A contribution to the design and the installation of an universal platform of a wind emulator using a dc motor', *Int. J. Renew. Energy Res.*, 2012, **2**, (4), pp. 797–804

[30] Slootweg, J., De Haan, S., Polinder, H., *et al.*: 'General model for representing variable speed wind turbines in power system dynamics simulations', *IEEE Trans. Power Syst.*, 2003, **18**, (1), pp. 144–151

[31] Ackermann, T.: '*Wind power in power systems*', vol. 140 (Wiley Online Library, Chichester, England, 2005)

[32] Slootweg, J., Polinder, H., Kling, W.: 'Representing wind turbine electrical generating systems in fundamental frequency simulations', *IEEE Trans. Energy Convers.*, 2003, **18**, (4), pp. 516–524

[33] Heier, S.: '*Grid integration of wind energy: onshore and offshore conversion systems*' (John Wiley & Sons, Chichester, England, 2014)

[34] Wasynczuk, O., Man, D., Sullivan, J.: 'Dynamic behavior of a class of wind turbine generators during randon wind fluctuations', *IEEE Trans. Power Appar. Syst.*, 1981, **6**, pp. 2837–2845

[35] Ofualagba, G., Ubeku, E.: 'Wind energy conversion system-wind turbine modeling'. 2008 IEEE Power and Energy Society General Meeting-Conversion and Delivery of Electrical Energy in the 21st Century IEEE, Pittsburgh, PA, USA., 2008, pp. 1–8

[36] El-Ahmar, M., El-Sayed, A.-H.M., Hemeida, A.: 'Evaluation of factors affecting wind turbine output power'. 2017 Nineteenth Int. Middle East Power Systems Conf. (MEPCON) IEEE, Cairo, Egipt, 2017, pp. 1471–1476

[37] Amlang, B., Arsurdis, D., Leonhard, W., *et al.*: 'Elektrische energieversorgung mit windkraftanlagen', Abschlußbericht BMFT Forschungsvorhaben, 1992, 032–8265

[38] Dai, J., Hu, Y., Liu, D., *et al.*: 'Modelling and analysis of direct-driven permanent magnet synchronous generator wind turbine based on wind-rotor neural network model', *Proc. Inst. Mech. Eng. A, J. Power Energy*, 2012, **226**, (1), pp. 62–72

[39] Chalise, S., Atia, H.R., Poudel, B., *et al.*: 'Impact of active power curtailment of wind turbines connected to residential feeders for overvoltage prevention', *IEEE Trans. Sust. Energy*, 2015, **7**, (2), pp. 471–479

[40] Yilmaz, A.S., Özer, Z.: 'Pitch angle control in wind turbines above the rated wind speed by multi-layer perceptron and radial basis function neural networks', *Expert Syst. Appl.*, 2009, **36**, (6), pp. 9767–9775

[41] Murdoch, A., Winkelman, J., Javid, S., *et al.*: 'Control design and performance analysis of a 6 mw wind turbine-generator', *IEEE Trans. Power Appar. Syst.*, 1983, **5**, pp. 1340–1347

[42] Abdin, E.S., Xu, W.: 'Control design and dynamic performance analysis of a wind turbine-induction generator unit', *IEEE Trans. Energy Convers.*, 2000, **15**, (1), pp. 91–96

[43] Betz, A.: 'Das maximum der theoretisch Möglichen ausnutzung des windes durch windmotoren', *Z. Turbinen.*, 1920, **20**, pp. 307–309

[44] Kaltschmitt, M., Streicher, W., Wiese, A.: '*Renewable energy, technology, economics and environment*' (Springer, Berlin, Germany, 2007)

[45] Miller, N.W., Price, W.W., Sanchez-gasca, J.J.: 'Dynamic Modeling of GE 1.5 and Prepared and 3.6 Wind Turbine-Generators', GE-Power Systems Energy Consulting, 2003

[46] Dai, J., Liu, D., Wen, L., *et al.*: 'Research on power coefficient of wind turbines based on scada data', *Renew. Energy*, 2016, **86**, pp. 206–215

[47] Asghar, A.B., Liu, X.: 'Estimation of wind turbine power coefficient by adaptive neuro-fuzzy methodology', *Neurocomputing*, 2017, **238**, pp. 227–233

[48] Qu, H., Hu, J., Gao, X.: 'The impact of Reynolds number on two-dimensional aerodynamic airfoil flow'. 2009 World Non-Grid-Connected Wind Power and Energy Conf. IEEE, Nanjing, China, 2009, pp. 1–4

[49] Buhl, Jr. M.L.: 'New empirical relationship between thrust coefficient and induction factor for the turbulent windmill state', Technical report, National Renewable Energy Lab.(NREL), Golden, CO (United States), 2005

[50] Jonkman, J., Butterfield, S., Musial, W., *et al.*: 'Definition of a 5-mw reference wind turbine for offshore system development', Technical report, National Renewable Energy Lab.(NREL), Golden, CO (United States), 2009

[51] Bak, C., Zahle, F., Bitsche, R., *et al.*: 'The DTU 10-MW reference wind turbine', Danish Wind Power Research 2013, 2013

[52] Bak, C., Bitsche, R., Yde, A., *et al.*: 'Light rotor: the 10-MW reference wind turbine'. EWEA 2012-European Wind Energy Conf. & Exhibition European Wind Energy Association (EWEA), Copenhagen, Denmark, 2012

[53] Hau, E., Langenbrinck, J., Palz, W.: '*WEGA large wind turbines*' (Springer Science & Business Media, Berlin, Germany, 2013)

[54] Soraperra, G.: 'Analysis on aerodynamic and aeroelastic behaviour of a wind turbine rotor during icing', PhD thesis, Technical University of Denmark, Citeseer, 2005

[55] Shalev-Shwartz, S., Ben-David, S.: 'Understanding machine learning: From theory to algorithms', Vol. 9781107057135, 2013. Available at https://doi.org/10.1017/CBO9781107298019 doi: 10.1017/CBO9781107298019

[56] Dan Foresee, F., Hagan, M.T.: 'Gauss-newton approximation to bayesian learning'. IEEE Int. Conf. on Neural Networks - Conf. Proc., Houston, TX, USA., 1997, vol. 3, pp. 1930–1935. Available at https://doi.org/10.1109/ICNN.1997.614194, doi: 10.1109/ICNN.1997.614194